The MS-Q Force Field for Clay Minerals: Application to Oil Production

Sungu Hwang,† Mario Blanco, Ersan Demiralp, Tahir Cagin, and William A. Goddard, III*

Materials and Process Simulation Center, Beckman Institute (139-74), Division of Chemistry and Chemical Engineering, California Institute of Technology, Pasadena, California 91125

Received: July 19, 2000; In Final Form: December 18, 2000

A Morse-charge equilibration force field (MS-Q FF), originally developed for the bulk oxides SiO_2 and Al_2O_3, has been used to model kaolinite and pyrophyllite clay minerals and their interactions with representative organic molecules. The MS-Q FF reproduces the structural parameters for these clay minerals and gives accurate enthalpies of immersions in water, organic solvents, and hydrocarbons. To form a basis for improving squeeze corrosion treatment strategies, we calculate the adsorption energy of oleic imidazoline, a corrosion inhibitor oil production chemical.

1. Introduction

Molecular modeling studies of clay and related zeolite structures were initially focused on structural and chemical reactivity issues. These included ab initio molecular orbital studies of the effects of basis set size on the calculated structure and acidity of hydroxyl groups in framework molecular sieves,[1,2] the modeling of the clay−water interface [3], clay hydration,[4] and the role of ions in swelling.[5] The molecular dynamics of clay minerals has been more recently undertaken for gibbsite, kaolinite, pyrophyllite, and beidellite.[6] Enthalpies of adsorption for hydrocarbons on smectite clay[7] and trichloroethene in kaolinite and pyrophyllite[8] humic substances in soils (oxidized lignins)[9] from molecular modeling calculations have been reported. A test of commercial force fields for the modeling of aniline vermiculite and tetramethylammonium vermiculite has been reported.[10] Here we report on the use of a new force field for the structural studies and adsorption thermodynamics of water, hydrocarbons, and polar organic compounds such as oil field production chemicals on clay mineral surfaces.

In parallel, significant progress has been made on the application of molecular simulations in studying oil production chemicals, including corrosion inhibitors,[11] scale inhibitors,[12] and dissolvers.[13] So far, the focus has been on the mechanism by which these oil field chemicals act to inhibit corrosion and scale. Thus, we have considered the interaction between these chemicals with their target materials (barite crystals for scale inhibitors and scale dissolvers or mild steel surfaces for corrosion inhibitors). However, it is also necessary to consider the interaction of these oil field additives with the reservoir rock surfaces. Of particular interest is the ability to tune the strength of the molecular sorption processes into the formation rock so as to increase the time period over which oil production additives are kept at the appropriate concentration in the oil (squeeze treatments for scale control and corrosion inhibition).

Among the minerals present in the walls of oil reservoirs, clay minerals are believed to be the most important because of their specific surface area and electric charge density. The sorption of oil field chemicals on clays and the slow release of the chemicals into the reservoir are important in determining the lifetime of the inhibitor. A better understanding of the interaction between clays and these chemicals is necessary to unravel the mechanism of squeeze treatments, to evaluate the treatment lifetime, and to make the optimum choice of a treatment strategy based on rock mineral composition.

Understanding the interaction between organic molecules and clay minerals is also important in other areas. An important one is enhanced oil recovery processes. Surface energies and the water and oil wettabilities of the exposed clay minerals are of great importance in heavy oil retention processes. Adsorption of polar compounds, such as asphaltenes, greatly affects the wetting properties of clays and, thus, the production capacity of the reservoir over time. Consequently, the simulation of the adsorption of squeeze treatment chemicals and hydrocarbons on clay minerals, which directly addresses the mechanisms of retention by the reservoir rock formation, should help evaluate crude oil recovery expectations and improve the ability to choose suitable oil recovery and field treatment strategies.

2. Force Field Parameter for Clay

We begin with the MS-Q force field (FF) developed for describing bulk SiO_2 and Al_2O_3 systems by Demiralp et al.[14−17] This FF allows the atomic charges to readjust as a function of the instantaneous geometry using the charge equilibration (QEq) procedure[18] of Rappé and Goddard. In addition to electrostatic interactions, MS-Q uses a two-body Morse function to describe nonelectrostatic terms

$$E_{ij}^{\mathrm{Morse}}(R_{ij}) = D_0\left\{\exp\left[-\gamma\left(\frac{R_{ij}}{R_0}-1\right)\right]-2\exp\left[-\frac{\gamma}{2}\left(\frac{R_{ij}}{R_0}-1\right)\right]\right\} \quad (1)$$

The parameters for Si, O, and Al were taken from the previous work for the silicate and aluminophosphate.[14−17] The FF parameters for hydrogen were optimized to reproduce the structural parameters for kaolinite and pyrophyllite. The optimized parameters are listed in Table 1 and Table 2. This type of force field has been successfully applied to predict structural changes upon external pressure loads on the polymorphism of silicates and aluminophosphates.[14−17]

* Corresponding author.
† Present Address: School of Chemistry, Seoul National University, Seoul 151-747, Korea.

10.1021/jp002570r CCC: $20.00
Published on Web 04/17/2001

TABLE 1: Diagonal Morse-Type van der Waals Potential

atom types	R_o	D_o	γ	note
H_C	3.3472	0.3796×10^{-4}	12.0000	hydrogen
O_3C[a]	3.7835	0.5363	10.4112	oxygen(hydrogen bonding donor)
O_AC[a]	3.7835	0.5363	10.4112	oxygen(hydrogen bonding acceptor)
Al3C[a]	3.8915	0.3321	11.9071	aluminum
Si3C[a]	3.4103	0.2956	11.7139	silicon

[a] These force field parameters are taken from refs 14−17.

TABLE 2: Off-Diagonal Morse-Type van der Waals Potential

atom types	R_o	D_o	γ
O_AC ... O_3C[a]	3.7835	0.5363	10.4112
Al3C ... O_3C[a]	1.7775	26.03	9.7830
Al3C ... O_AC[a]	1.7775	26.03	9.7830
Si3C ... O_3C[a]	1.6248	46.00	8.3022
Si3C ... O_AC[a]	1.6248	46.00	8.3022
O_3C ... H_C	1.0770	19.55	8.4394
O_AC ... H_C	2.1768	0.1753	16.0000
Si3C ... Al3C[a]	4.0949	0.0000	8.7732

[a] These force field parameters are taken from reference.[14−17]

TABLE 3: Comparison of the Optimized Structure of Kaolinite with the Experimental Neutron Scattering Data

	this work (MM)	exp. (1.5K)[a]
a (Å)	5.095	5.1535
b (Å)	8.840	8.9419
c (Å)	7.567	7.39036
density (g/cm^3)	2.607	2.60835
O(donor)−H (Å)	1.02	0.977
O(acceptor)−H (Å)	2.22	2.2005
RMS deviation from exp. (Å)	0.118 (0.116[b])	

[a] Ref 19. [b] For non-hydrogen atoms.

TABLE 4: Comparison of the Optimized Structure of Pyrophyllite with the X-Ray Data

	this work (MM)	exp. (X-ray)[a]
a (Å)	5.119	5.160
b (Å)	8.905	8.966
c (Å)	9.214	9.347
density (g/cm^3)	2.898	2.815
RMS deviation from exp. (Å)	0.07[b]	

[a] Ref 20. [b] For non-hydrogen atoms.

Kaolinite has a 1:1 layered structure, with one silicate tetrahedral sheet alternating with one octahedral sheet. Pyrophyllite is of a dioctahedral 2:1 type which has 2 tetrahedral sheets and 1 octahedral sheet (ideal model for mica and dioctahedral structures). The crystal structure parameters for kaolinite were taken from the neutron scattering experiments of Bish performed at 1.5 K.[19] Those of pyrophyllite were taken from the X-ray experiment of Lee and Guggenheim for one layer triclinic (1Tc) form.[20]

3. Results: Structure of Clays

The simulation results for kaolinite and pyrophyllite are in excellent agreement with the neutron scattering[19] (kaolinite) and X-ray crystallographic[20] (pyrophyllite) experiments, as shown in Tables 3 and 4. The MS-Q optimized structures are shown in Figure 1.

4. Adsorption Enthalpies for Hydrocarbons on Clay

The sorption of hydrocarbons on clay surfaces is the key to the use of clays in the discovery, recovery, and processing of petroleum. Consequently, it is important to ensure that such interactions are modeled with high accuracy. To validate the FF, we performed molecular mechanics studies of the enthalpies of adsorption of 13 linear, branched, and cyclic aliphatic hydrocarbons on the surface of pyrophyllite clay and compared the results with experiments[21,22] performed for smectite montmorillonite, a closely related dioctahedral smectite mineral. The heats of adsorption were taken from gas chromatographic retention volumes measured at 423 K. At this relatively high temperature, it is considered that nearly all the interlayer water has been removed and that the clay layers are collapsed to just the size of the interlayer cation. Therefore, it is reasonable to assume that the hydrocarbon uptake is minimal within the interlayer and that water and inner-layer cations need not be included in the simulation.[22]

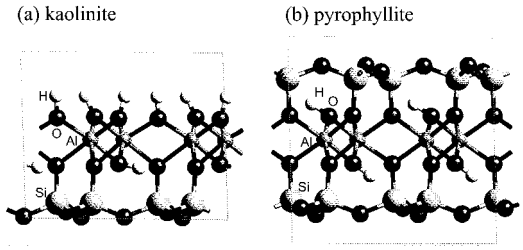

Figure 1. MM optimized structures of (a) kaolinite and (b) pyrophyllite.

To model the external clay surface, we used the $4 \times 2 \times 1$ superlattice of pyrophyllite, which is the ideal model for the 2:1 dioctahedral smectite mineral groups. The *c* axis was extended so that the interlayer spacing was 20 Å, thus, the model effectively represents the external clay surface. The structures of adsorbates were optimized with the Dreiding II FF [23] (using the exponential-6 form for the van der Waals interactions). The atomic charges of the adsorbates were assigned using the charge equilibration (QEq) procedure.[18] The interactions between hydrocarbon adsorbate and clay were described using electrostatic interactions plus standard combination rules for van der Waals (vdW) interaction. The force field parameters for off-diagonal vdW terms are listed in Table 5, where the energy is represented by the following equation:

$$E_{\mathrm{vdw}}(R) = D_0\left\{\left[\left(\frac{6}{\zeta-6}\right)\exp^{\zeta(1-R/R_0)}\right] - \left[\left(\frac{\zeta}{\zeta-6}\right)\left(\frac{R_0}{R}\right)^6\right]\right\} \quad (2)$$

The results from molecular mechanics (MM) minimizations are listed in Table 6 and plotted in Figure 2. The results show a high correlation coefficient ($R^2 = 0.97$) between experimental and calculated values, which suggests that our FF reproduces the experimental binding energies and that the interactions between hydrocarbon and clay is of nonbonding character.

We analyzed further the binding energy with a group additive approach to obtain a simple equation for adsorption energies of hydrocarbons on clay surfaces (see Figure 3). The least-squares fitting to the energy of adsorption obtained from MM gives

$$E_{\mathrm{adsorption}} = -2.691n(\mathrm{CH_3}) - 2.049n(\mathrm{CH_2}) - 0.418n(\mathrm{CH}) + 1.498n(\mathrm{C}) \qquad R^2 = 0.991 \quad (3)$$

where $E_{\mathrm{adsorption}}$ is the energy of adsorption per adsorbate molecule (in kcal/mol), $n(\mathrm{CH_3})$ is the number of methyl carbons in the adsorbate, $n(\mathrm{CH_2})$ the number of methylene carbons, and so on. This equation allows us to evaluate the energy of

TABLE 5: Off-Diagonal van der Waals Parameters for Clay−Organic and Clay−Water Interactions[a]

atom *i*	atom *j*	R_o	D_o	ζ
H_C	H_	3.1950	0.0152	12.3820
H_C	C_3	3.5392	0.0376	13.2285
H_C	N_3	3.4315	0.0338	13.1348
H_C	C_R	3.5392	0.0376	13.2285
H_C	N_R	3.4315	0.0338	13.1348
H_C	O_3	3.3043	0.0378	12.9456
O_3C	H_	3.3043	0.0378	12.9456
O_3C	C_3	3.6368	0.0964	13.7475
O_3C	N_3	3.5298	0.0862	13.6609
O_3C	C_R	3.6368	0.0964	13.7475
O_3C	N_R	3.5298	0.0862	13.6609
O_3C	O_3	3.4046	0.0957	13.4830
O_AC	H_	3.3043	0.0378	12.9456
O_AC	C_3	3.6368	0.0964	13.7475
O_AC	N_3	3.5298	0.0862	13.6609
O_AC	C_R	3.6368	0.0964	13.7475
O_AC	N_R	3.5298	0.0862	13.6609
O_AC	O_3	3.4046	0.0957	13.4830
Al3C	H_	3.6245	0.0821	11.9769
Al3C	C_3	4.0863	0.1853	12.9405
Al3C	N_3	3.9267	0.1751	12.7884
Al3C	C_R	4.0863	0.1853	12.9405
Al3C	N_R	3.9267	0.1751	12.7884
Al3C	O_3	3.7463	0.2059	12.5384
Si3C	H_	3.5927	0.0799	12.0101
Si3C	C_3	4.0447	0.1816	12.9640
Si3C	N_3	3.8895	0.1709	12.8166
Si3C	C_R	4.0447	0.1816	12.9640
Si3C	N_R	3.8895	0.1709	12.8166
Si3C	O_3	3.7136	0.2002	12.5716
H_C	H_F	3.1950	0.0152	12.3820
H_C	O_3F	3.3043	0.0378	12.9456
O_3C	H_F	3.3043	0.0378	12.9456
O_3C	O_3F	3.4046	0.0957	13.4830
O_AC	H_F	3.3043	0.0378	12.9456
O_AC	O_3F	3.4046	0.0957	13.4830
Al3C	H_F	3.6245	0.0821	11.9769
Al3C	O_3F	3.7463	0.2059	12.5384
Si3C	H_F	3.5927	0.0799	12.0101
Si3C	O_3F	3.7136	0.2002	12.5716

[a] H_, hydrogen; C_3, sp^3 carbon; N_3, sp^3 nitrogen; C_R, carbon in pyridine; N_R, nitrogen in pyridine; O_3, sp^3 oxygen; H_F, hydrogen in water; O_F, oxygen in water.

adsorption of any linear or branched hydrocarbon on clay surfaces. Values for a few important hydrocarbons are listed in Table 6.

5. Heats of Immersion into Solvents

The heat of immersion of a clay mineral is closely related to its wetting properties. These values of practical importance in secondary and enhanced oil recovery processes. The free energy of immersion and the enthalpy of immersion can be defined as follows:[24]

$$\Delta_{imm}G = \gamma_{sl} - \gamma_s \tag{4}$$

$$\Delta_{imm}H = \Delta_{imm}G - T\left[\frac{\partial(\Delta_{imm}G)}{\partial T}\right]_P \tag{5}$$

where the γ_{sl} is the interfacial tension between solid and liquid solvent and γ_s is the surface tension of the solid.

In this study, heats of immersion of the kaolinite mineral were calculated from molecular dynamics (MD) simulations of the interfacial energy of the solvent/kaolinite and the surface energy

TABLE 6: Experimental and Calculated Enthalpies of Adsorption (kcal/mol)

	hydrocarbon	ΔE (MM)[a]	ΔH (exp, 423K)[b]	error	ΔE (fit)[c]
1	2-methylbutane	−11.08	−12.3	1.2	−10.54
2	cyclohexane	−12.36	−12.8	0.4	−12.29
3	pentane	−11.58	−13.5	1.4	−11.53
4	2-methylpentane	−11.90	−14.0	2.1	−12.59
5	hexane	−13.47	−15.3	1.8	−13.58
6	2,4-dimethylpentane	−13.65	−16.0	2.3	−13.65
7	3-methylhexane	−14.89	−16.3	1.4	−14.64
8	2,2,4-trimethylpentane	−14.43	−17.2	2.8	−14.43
9	heptane	−15.54	−17.4	1.8	−15.63
10	3-methylheptane	−16.58	−18.8	2.2	−16.69
11	octane	−18.02	−19.9	1.9	−17.67
12	nonane	−19.42	−21.7	2.3	−19.72
13	decane	−21.88	−23.7	1.8	−21.77

[a] An isolated molecule on the surface of a 4 × 2 × 1 unit cell. [b] Low-coverage limit from refs 21 and 22. [c] Based on eq 3.

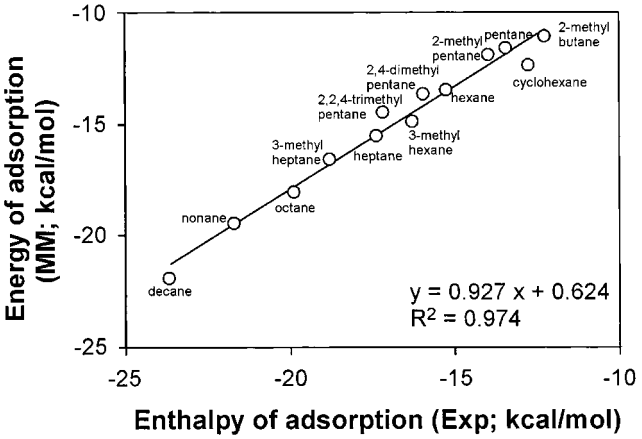

Figure 2. Plot of calculated heats of adsorption from energy minimization vs experimental values.

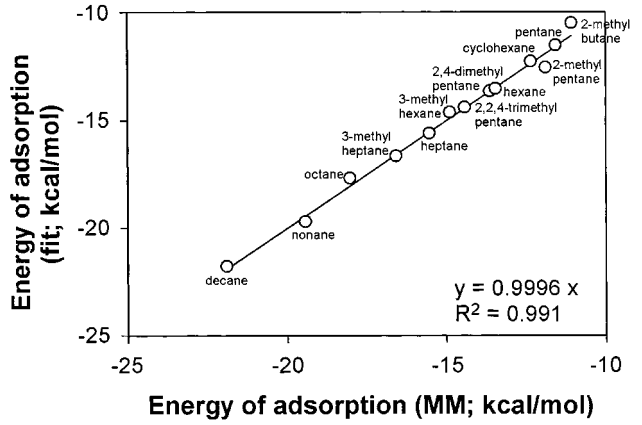

Figure 3. Plot of calculated heats of adsorption from least-squares fitting vs those from energy minimization.

of the exposed kaolinite mineral

$$\Delta_{imm}H = \Delta\langle E\rangle_{interface} - \Delta\langle E\rangle_{surface} \tag{6}$$

$$\Delta\langle E\rangle_{interface} = \frac{\Delta\langle E\rangle_{solid/solvent} - \Delta\langle E\rangle_{solid} - \Delta\langle E\rangle_{solvent}}{2S} \tag{7}$$

$$\Delta\langle E\rangle_{surface} = \frac{\Delta\langle E\rangle_{surface} - \Delta\langle E\rangle_{solid}}{2S} \tag{8}$$

where brackets signify the average over MD trajectories and S is the surface area.

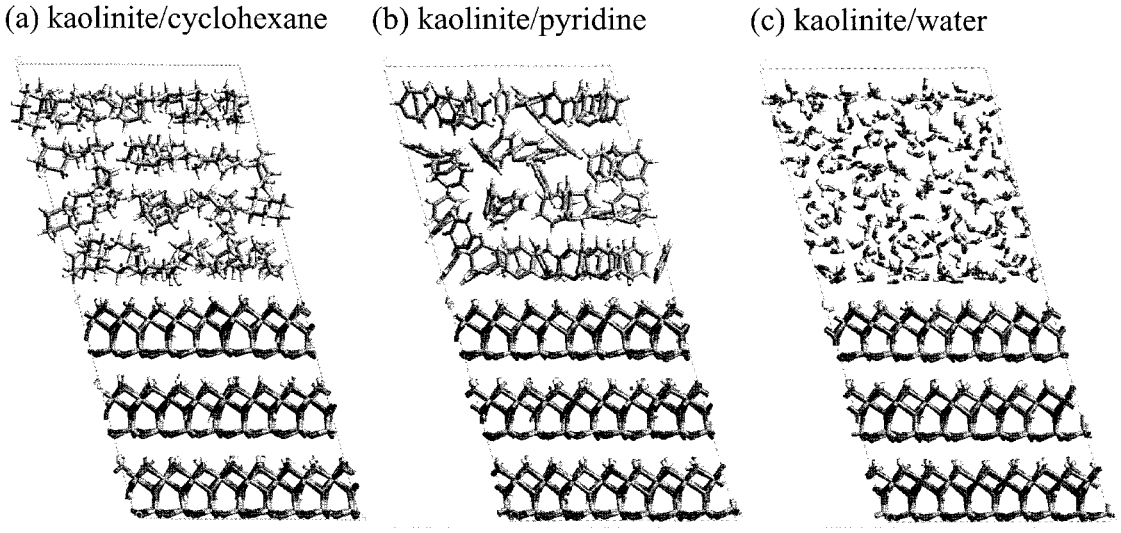

Figure 4. Typical snapshots from MD simulations: (a) kaolinite/cyclohexane, (b) kaolinite/pyridine, and (c) kaolinite/water. Kaolinite is represented as three layers. Note that the figures are the side view of the simulation box, and only one repeating unit is depicted.

TABLE 7: Heat of Immersion (mJ/m^2)

mineral	solvent	exp.	MM	MD
kaolinite	cyclohexane	−53[a]	−144	−122 ± 3
kaolinite	pyridine	−389 to −405[b]	−259	−238 ± 4
kaolinite	water	−196[a]	−176	−179 ± 3
		−480 to −485[c]		
pyrophyllite	cyclohexane	N/A	−175	−150 ± 2

[a] Ref 29. [b] Ref 30. [c] Ref 31.

We used the (001) surface of kaolinite with a (4 × 2 × 3) superlattice to represent the surface. We considered three solvents: cyclohexane, pyridine, and water, chosen to represent apolar, polar, and aqueous environments, respectively. The organic solvents were described using the Dreiding (II) FF[23] while water was described using the F3C water potential.[25] The atomic charges of cyclohexane were determined using QEq, while those of pyridine were obtained by fitting to the electrostatic potential obtained from the charge distribution in ab initio HF 6-31G** calculations. The charges for water were taken from the F3C potential.[25]

We carried out NVT MD simulations. The temperature was set to 300 K using the Nosé−Hoover thermostat.[26] The time step was set to 1 fs, and the length of the simulation was adjusted to ensure thermal equilibration and proper sampling. This procedure led to 25 ps for the pyridine and cyclohexane samples and 200 ps for the water box and mineral/water composite system. The potential energy is reported as the average of three or four block averages after equilibration. The results are summarized in Table 7, which lists the heat of immersion calculated by molecular mechanics and MD.

In Figures 4 and 5, we present typical time snapshots from the MD simulations, providing dynamic structural information of the clay minerals immersed in solvents. At the boundaries between solution and clay layers, the solvent molecules are aligned to maximize the interactions with the clay surfaces. As seen in Figures 4 and 5, this alignment is maintained roughly over a single layer. The solvent molecules are randomly oriented in the bulk solvent. The orientation of the cyclohexane at the interfaces is random for both silica and alumina sheets. However, pyridine is aligned so that nitrogen and hydrogen atoms are near the alumina and silica sheets, respectively. For the kaolinite/water system, the water oxygen atoms are near the alumina sheet, and the hydrogen atoms are positioned near the silica sheet.

6. Adsorption Energies of Imidazoline on Clay Surfaces

As an application of the newly developed clay mineral FF, we calculated the adsorption of imidazoline on clay surfaces. Imidazolines are inhibitors of mild steel corrosion in oil field applications. A self-assembled monolayer (SAM) model was proposed and successively applied to explain the action of the inhibitor.[11] As a model, we chose a simple imidazoline **1** (OI-2-CCN, see ref 11 for notation). Imidazoline **1** was adsorbed on the two surfaces, alumina and silica, of kaolinite. We employed MM calculations for different coverages: 1, 2, 4, and 8 molecules on (3 × 2 × 3) and (4 × 2 × 3) surfaces. The binding energies are plotted as a function of surface coverage. From the least-squares fitting of the energy, we can define the adsorption energy at infinite dilution (denoted as $E_{ads-surface}$) as the *y*-intercept of the curve (See Figure 6). The analysis gives −19.67 kcal/mol for the alumina sheet and −20.53 kcal/mol for the silica sheet. Further analysis of the structures confirms that imidazoline **1** prefers the silica sheet to alumina sheet. At high coverage a self-assembled structure ensues, but the binding of the adsorbate molecule is less favorable due to steric repulsion between adsorbates. A similar study on heptane on the surface of pyrophyllite (which resembles the silica sheet of kaolinite) gives −15.99 kcal/mol for $E_{ads-surface}$. These sorption energies clearly suggests that imidazoline can be successfully adsorbed on clay surfaces in an oil field. Furthermore, the sorption energies allow for transport of imidazoline to mild steel surfaces, where the binding energy was previously found to be much higher,[11] −41.8 kcal/mol.

7. Discussion

We have shown that with the appropriate choice of a force field, it is possible to model, through molecular dynamics calculations, not only the structural features of key clay minerals but also the sorption energetics of organic compounds, such as hydrocarbons, as well as the enthalpies of immersion of clays into polar and nonpolar solvents. This provides some confidence that such calculations can be used to estimate sorption energetics of oil additives such as scale-control chemicals (polyamino-acetates and polyaminophosphonates), and corrosion inhibitors (oleic imidazolines).

On the basis of the mineral rock composition of a specific reservoir, one can envision the optimal choice of these additives for extended retention times, gradual release, at a minimal

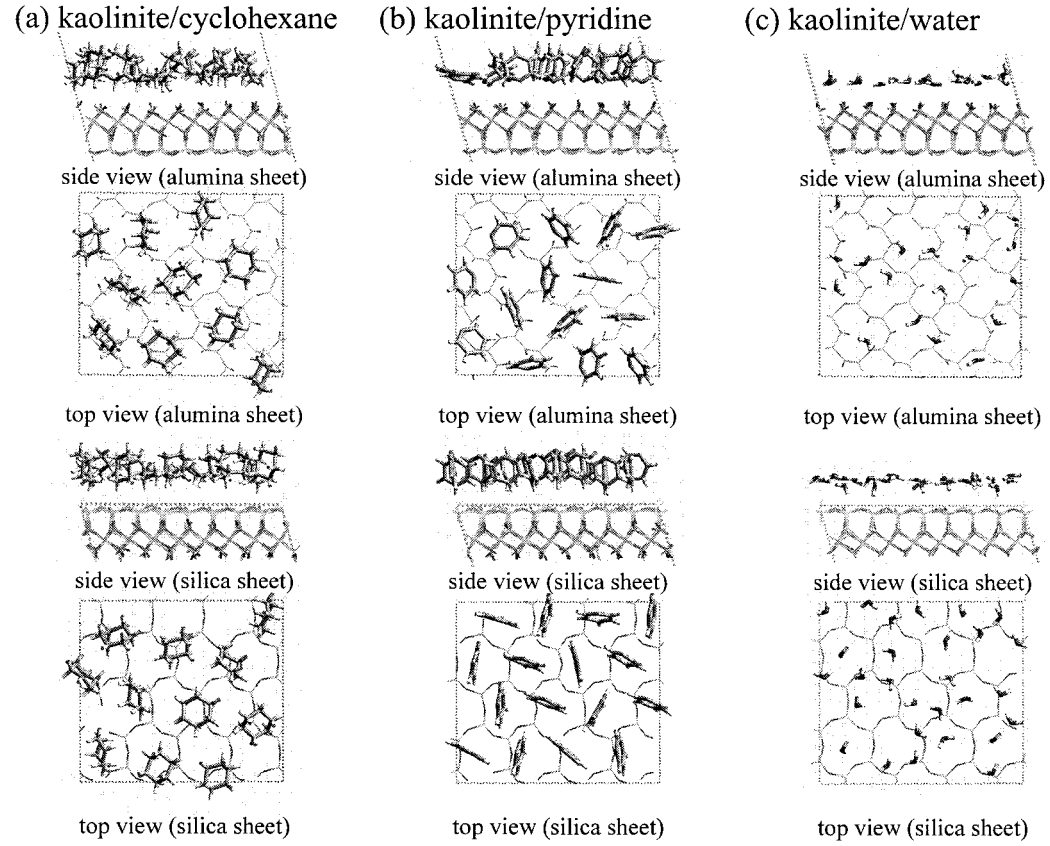

Figure 5. Typical snapshots for the clay/solvent interfaces from MD simulations: (a) kaolinite/cyclohexane, (b) kaolinite/pyridine, and (c) kaolinite/water. From top to bottom: side view for alumina sheet, top view for alumina sheet, side view for silica sheet, and top view for silica sheet. Only the solvents near the interfaces and one clay layer are depicted for clarity.

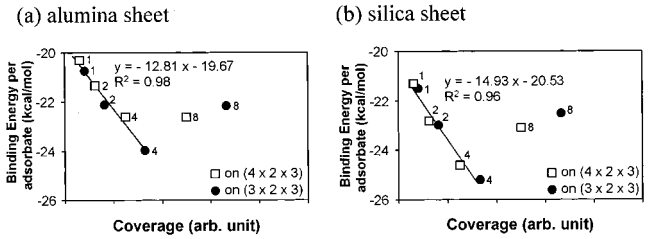

Figure 6. The binding energy per adsorbate molecule, imidazoline **1** on (a) alumina sheet and on (b) silica sheet of Kaolinite (001) surface. Filled circle denotes the adsorption on (3 × 2 × 3) superlattice and square denotes (4 × 2 × 3). The number beside the symbol is the number of adsorbate molecules per unit cell of a superlattice.

environmental impact. Furthermore, one may use the insight gained from these simulations to help developed enhanced recovery procedures (such as surfactant and chemical flooding compounds) for heavy oils. The molecular dynamics of oil and water phase flow over chemically modified clay surfaces can form the basis for a rational design of hydrodynamic surface modifiers in the same way that the modeling of organic additives on metal surfaces has helped the discovery of novel metal wear inhibitors.[27,28]

Clays in nature are usually covered with other minerals and organic substances, organic-cementing agents, consisting of proteinaeceous and humic materials,[32] C_6-C_{30} methyl esters of aliphatic and aromatic acids, and methoxy derivatives of phenols and phenolic acids.[33] In real reservoir applications, these compounds must be taken into account. We have presented here a new clay force field and a general method which might yield useful predictions for such complex sorption equilibrium.

Acknowledgment. This research was initially funded by Saudi Aramco, continued under funding by Chevron Petroleum Technology Co., and completed under funding by the National Petroleum Office (NPTO) of the Department of Energy. Additional support for the facilities of the MSC was also provided by grants from DOE-ASCI, NSF (CHE 95-12279), BP Chemical, ARO-MURI, ARO-DURIP, the Beckman Institute, Exxon, Avery Dennison, 3M, Dow, General Motors, Kellogg, and Asahi Chemical.

References and Notes

(1) Nicholas, J. B.; Winans, R. E.; Harrison, R. J.; Iton, L. E.; Curtiss, L. A.; Hopfinger, A. J. *J. Phys. Chem.* **1992**, *96*, 10247.

(2) Nicholas, J. B.; Winans, R. E.; Harrison, R. J.; Iton, L. E.; Curtiss, L. A.; Hopfinger, A. J. *J. Phys. Chem.* **1992**, *96*, 7958.

(3) Delville, A. *Langmuir* **1991**, *7*, 547.

(4) Boek, E. S.; Coveney, P. V.; Skipper, N. T. *Langmuir* **1995**, *11*, 4629.

(5) Boek, E. S.; Coveney, P. V.; Skipper, N. T. *J. Am. Chem. Soc.* **1995**, *117*, 12608.

(6) Teppen, B. J.; Rasmussen, K.; Bertsch, P. M.; Miller, D. M.; Schafer, L. *J. Phys. Chem. B* **1997**, *101*, 1579.

(7) Keldsen, G. L.; Nicholas, J. B.; Carrado, K. A.; Winans, R. E. *J. Phys. Chem.* **1994**, *98*, 279.

(8) Teppen, B. J.; Yu, C. H.; Miller, D. M.; Schafer, L. *J. Comput. Chem.* **1998**, *19*, 144.

(9) Shevchenko, S. M.; Bailey, G. W.; Akim, L. G. *THEOCHEM* **1999**, *460*, 179.

(10) Capkova, P.; Burda, J. V.; Weiss, Z.; Schenk, H. *J. Mol. Model.* **1999**, *5*, 8.

(11) Ramachandran, S.; Tsai, B. L.; Blanco, M.; Chen, H.; Tang, Y.; Goddard, W. A., III *J. Phys. Chem. A* **1997**, *101*, 83.

(12) Jang, Y. H.; Blanco, M.; Tang, Y.; Shuler, P.; Goddard, W. A., III. Manuscript in preparation.

(13) Blanco, M.; Tang, Y.; Shuler, P.; Goddard, W. A., III. *J. Mol. Eng.* **1997**, *7*, 491.

(14) Cagin, T.; Demiralp, E.; Goddard, W. A., III. Pressure Induced Phase Transformations in Silica. In *Microscopic Simulation of Interfacial Phenomena in Solids and Liquids*; Symposia Series 492; Phillpot, S. R., Bristowe, P. D., Stroud, D. G., Smith, J. R., Eds.; Materials Research Society: Pittsburgh, 1998; p 287.

(15) Demiralp, E.; Cagin, T.; Goddard, W. A., III. *Phys. Rev. Lett.* **1999**, *82*, 1708.

(16) Kitao, O.; Demiralp, E.; Cagin, T.; Dasgupta, S.; Mikami, M.; Tanabe, K.; Goddard, W. A., III. *Comput. Mater. Sci.* **1999**, *14*, 135.

(17) Demiralp, E.; Cagin, T.; Huff, N. T.; Goddard, W. A., III The MS-Q Force Fields for Metal Oxides. Manuscript to be submitted.

(18) Rappé, A. K.; Goddard, W. A., III. *J. Phys. Chem.* **1991**, *95*, 3358.

(19) Bish, D. L. *Clays Clay Mineral.* **1993**, *41*, 738.

(20) Lee, J. H.; Guggenheim, A. S. *Am. Mineral.* **1981**, *66*, 350.

(21) Zhukova, A. I.; Bondarenko, S. V.; Tarasevich, Y. I. *Ukr. Khim. Zh.* **1976**, *42*, 708.

(22) Keldsen, G. L.; Nicholas, J. B.; Carrado, K. A.; Winans, R. E. *J. Phys. Chem.* **1994**, *98*, 279.

(23) Mayo, S. L.; Olafson, B. D.; Goddard, W. A., III *J. Phys. Chem.* **1990**, *94*, 8897.

(24) Lagerge, S.; Rousset, P.; Zoungrana, T.; Douillard, J. M.; Partyka, S. *Colloids Surf. A* **1993**, *80*, 261.

(25) Levitt, M.; Hirshberg, M.; Sharon, R.; Laidig, K. E.; Daggett, V. *J. Phys. Chem. B* **1997**, *101*, 5051.

(26) Hoover, W. G. *Phys. Rev. A* **1985**, *31*, 1695.

(27) Jiang, S.; Dagsupta, S.; Blanco, M.; Frazier, R.; Yamaguchi, E. S.; Tang, Y.; Goddard, W. A., III. *J. Phys. Chem.* **1996**, *100*, 15760.

(28) Jiang, S.; Frazier, R.; Yamaguchi, E. S.; Blanco, M.; Dasgupta, S.; Zhou, Y.; Cagin, T.; Tang, Y.; Goddard, W. A., III. *J. Phys. Chem. B* **1997**, *101*, 7702.

(29) Partyka, S.; Douillard, J. M. *J. Petroleum Sci. Eng.* **1995**, *13*, 95.

(30) Zoungrana, T.; Berrada, A.; Douillard, J. M.; Partyka, S. *Langmuir* **1995**, *11*, 1760.

(31) Partyka, S.; Rouquerol, F.; Rouquerol, J. *J. Colloid Interface Sci.* **1979**, *68*, 21.

(32) Skjemstad, J.; Janik, J. L.; Head, M. J.; McClure, S. G. *J. Soil Sci.* **1993**, *44*, 15.

(33) Schulten, H. R.; Leinweber, P.; Theng, B. K. G. *Geoderma* **1996**, *69*, 14.